Hindawi
Mathematical Problems in Engineering
Volume 2018, Article ID 3094980, 12 pages
https://doi.org/10.1155/2018/3094980

Research Article

Exact Analytical Nanofluid Flow and Heat Transfer Involving Asymmetric Wall Heat Fluxes with Nonlinear Velocity Slip

Jing Zhu, Pengfei Chu, and Jiani Sui

Department of Applied Mathematics, University of Science and Technology Beijing, 100083 Beijing, China

Correspondence should be addressed to Jing Zhu; zhujing@ustb.edu.cn

Received 4 May 2018; Revised 7 August 2018; Accepted 14 August 2018; Published 16 September 2018

Academic Editor: Vincenzo Bianco

Nanofluid slip flow and heat transfer over the microchannel with asymmetric wall heat fluxes are investigated theoretically. The local thermal nonequilibrium model in which there is a difference between the solid temperature and nanofluid temperature is modified by considering the nonlinear velocity slip and temperature jump. Exact analytical solutions and homotopy series solutions for both velocity and temperature of nanofluid and solid are first obtained. Two groups of solutions agree well with existing references and residual errors are plotted. In addition, the effects of the physical factors on the heat transfer are graphically discussed. The results show that the first velocity slip enhances Nusselt numbers while the second slip coefficient has a reverse effect on them. As expected, the nanoparticle concentration enhances heat transfer on bottom wall.

1. Introduction

A nanofluid was put forward by Choi [1] of the U.S. Argonne National Laboratory in 1995. Due to enhancing the original fluid thermal physical property and strengthening the energy exchange of media, nanofluids have been applied in many fields. For example, the nanofluids were applied to the tidal energy technology [2] and used as the heat conduction medium [3]. Many researchers have also performed theoretical studies of heat transfer with nanofluids. Ghazvini and Shokouhmand [4] discussed nanofluid flow through a micropipeline and analyzed the effects of volume fraction on dispersion and thermal conductivity. Hatami [5] et al. subsequently found the influence of the size and type of nanoparticles upon the thermal behavior. Hooseini et al. [6] got the relationship between Nusselt number and the volume fraction. In addition, these authors found that increasing concentration of nanoparticles will improve the value of the Nusselt number.

Transfers in porous media also are significant research topics from engineering. Some works on nanofluid flow and heat transfer in porous media were conducted. Chamkha [7] et al. studied viscous dissipation and magnetic field effects on a Non-Darcy Porous Medium Saturated under Convective Boundary Condition. The temperatures of the solid and fluid phases are considered to be the same within the representative elementary volume based on the local thermal equilibrium (LTE). But LTE model has a low coefficient of Biot and people began to think that solid phase and nanofluids phase cannot be ignored in the porous medium. As a result, more and more scholars considered the Local Thermal Non-Equilibrium (LTNE) model [8, 9] to perform theoretical and experimental studies. Haddad et al. [10] used the LTNE Forchheimer model to simulate the forced convection porous in microchannel. Nojoomizadehet al. [11] numerically investigated permeability and porosity effects on heat transfer rate of Fe3O4/water nanofluid flow in a microchannel. The LTNE model also is applied in some areas such as electronics cooling, chemical and nuclear reactors, solar collectors, and fuel cells [12].

In addition to heat transfer analysis of nanofluids under the local thermal nonequilibrium condition, fluids exhibiting slip is important in technological applications such as in the polishing of artificial heart valves and internal cavities. Therefore, better understanding of the phenomenon of slip is necessary. Scientists have done an impressive account of research on nanofluids slip flow problems [13]. To mention a few of the active topics, forced convection in a parallel-plate

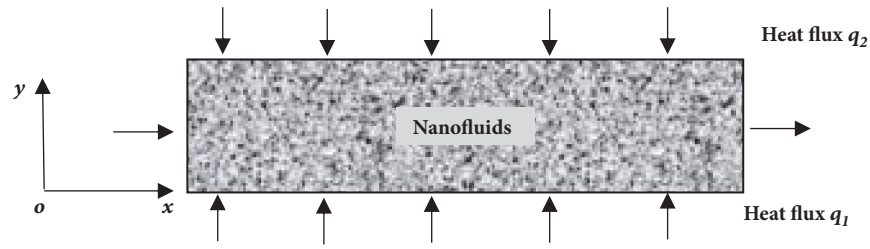

Figure 1: Schematic diagram of present problem.

porous microchannel based on slip flow model has been studied by Buonomo et al. [14]; slip flow forced convection in rectangular microduct filled with porous media has been studied by Hooman [15]; heat transfer through microfoams in microchannels with asymmetric wall heat flux has been studied by H. J. Xu et al. [16]. MHD mixed convection in a two-sided lid-driven porous cavity has been studied by Sivasankaran et al. [17]. In these investigations, the linear Navier's slip condition performs well at sufficiently low shear rate. However, the Navier's slip condition breaks down at higher shear rates as the slip length increases rapidly. Therefore, the concept of nonlinear slip boundary conditions is put forward. Thompson [18] developed a nonlinear slip model based on Maxwell's first-order slip model. Some researchers reported that Thompson's model cannot predict the flow in high Kn number and put forward a second-order slip conditions [19]. Comparison between calculation result and experimental data demonstrated that the values calculated by using second-order slip boundary conditions are closer to the experimental value. Zhu et al. [20] investigated analytically the effects of second-order velocity slip and nanoparticles migration on flow of Buongiorno nanofluid.

According to the literature and to the best knowledge of the authors, very limited investigation was given to the heat transfer with second-order slip velocity and temperature jump under the LTNE model. Given these, the current work aims to investigate theoretically a two-dimensional laminar flow and heat transfer of nanofluids through the microchannel with nonlinear velocity slip and temperature jump. Besides, the effects of nanofluids particles are discussed for nanofluids of porous media. Explicit analytical solutions and the semianalytical solution of the homotopy analysis are obtained.

2. Mathematical Modeling

Consider the slip flow and heat transfer in the porous microchannel with asymmetric boundary heat fluxes, as shown schematically in Figure 1. Distance between the two parallel-plates is H. Asymmetric constant heat flux q_1 and q_2 are imposed on the microchannel. For mathematically describing this problem, the following assumptions are invoked in the formulation of the model: The nanofluids flow in the porous medium are incompressible and corresponding homogeneous then the flow and heat transfer are fully developed. Heat generations due to viscous resistance are considered. Flow is subjected to a constant applied magnetic field in the direction of y-axis. The velocity slip and temperature jump are considered in the porous-solid boundary. In addition, the temperature of the solid and fluid phases can be different under the local thermal nonequilibrium model. The LTNE models are extended to nanofluids. Thermophysical properties such as porosity, specific heat, and concentration of nanoparticles and base fluid are constant. The thermophysical properties are given in Table 1. Consequently, the governing equations can be expressed in the following manner:

Table 1: Thermophysical properties of water with Cu, Fe_3o_4 nanoparticles.

Physical properties	Water	Cu	Fe_3o_4
ρ (kg/m3)	997.1	8954	5200
k (Wm−1 K−1)	0.613	400	6
c (J/kg K)	4179	383	670
σ $(\Omega m)^{-1}$	0.05	1.75∗10-8	4∗10-5

$$\frac{\mu_{nf}}{\varepsilon}\frac{\partial^2 u}{\partial y^2} = \frac{dp_{nf}}{dx} - \frac{\mu_{nf}}{K}u - \frac{\rho_{nf}CI}{\sqrt{K}}u^2 - \sigma_{nf}{B_0}^2 u \tag{1}$$

$$k_{se}\frac{\partial^2 T_s}{\partial y^2} - h_{sf}a_{sf}\left(T_s - T_{nf}\right) + S_s = 0 \tag{2}$$

$$k_{\mathrm{n}fe}\frac{\partial^2 T_{nf}}{\partial y^2} + h_{sf}a_{sf}\left(T_s - T_{nf}\right) + S_{nf} = \rho_{nf}c_{nf}u\frac{\partial T_{nf}}{\partial x} \tag{3}$$

Combined with second-order slip model, boundary conditions are

$$\begin{aligned} u &= \eta_v\frac{2-\sigma_v}{\sigma_v}\lambda\frac{\partial u}{\partial y} + \eta_v\frac{2-\sigma_v}{\sigma_v}\lambda^2\frac{\partial^2 u}{\partial y^2}, \\ T_s &= T_{w1}, \\ T_{nf} &= T_{w1} + \eta_T\frac{2-\sigma_T}{\sigma_T}\frac{2\gamma}{\gamma+1}\frac{\lambda}{\mathrm{Pr}}\frac{\partial T_{nf}}{\partial y} \\ &\quad + \eta_T\frac{2-\sigma_T}{\sigma_T}\frac{2\gamma}{\gamma+1}\frac{\lambda^2}{\mathrm{Pr}}\frac{\partial^2 T_{nf}}{\partial y^2}, \end{aligned} \tag{4}$$

$$y = 0$$

Table 2: Representative values based on different concentration rates.

ϕ	R_u	R_k	R_ρ	R_f	R_u	R_k	R_ρ	R_f
		Cu				Fe_3o_4		
0%	1.0	1.0	1.0	1.0	1.0	1.0	1.0	1.0
2.5%	1.0653	1.07656	1.19950	1.00002	1.06534	1.05975	1.10538	1.00053
5%	1.1368	1.15714	1.39900	1.00004	1.13682	1.11616	1.21076	1.00111

$$
\begin{aligned}
u &= -\eta_v \frac{2-\sigma_v}{\sigma_v}\lambda\frac{\partial u}{\partial y} \\
&\quad - \eta_v \frac{2-\sigma_v}{\sigma_v}\lambda^2\frac{\partial^2 u}{\partial y^2}, \\
T_s &= T_{w2}, \\
T_{nf} &= T_{w2} - \eta_T \frac{2-\sigma_T}{\sigma_T}\frac{2\gamma}{\gamma+1}\frac{\lambda}{\mathrm{Pr}}\frac{\partial T_{nf}}{\partial y} \\
&\quad - \eta_T \frac{2-\sigma_T}{\sigma_T}\frac{2\gamma}{\gamma+1}\frac{\lambda^2}{\mathrm{Pr}}\frac{\partial^2 T_{nf}}{\partial y^2}; \\
k_{se}\frac{\partial T_s}{\partial y} + k_{nfe}\frac{\partial T_{nf}}{\partial y} &= q_2, \\
& \qquad y = H
\end{aligned}
\tag{5}
$$

where η_v and η_T are corrective coefficients of velocity slip and thermal slip at the wall surface. σ_v and σ_T are, respectively, tangential momentum accommodation coefficient and thermal accommodation coefficient. Their value ranges are, respectively, about 0.6~1.0 and 0.0109~0.990[21].

In the fully developed area and constant boundary heat fluxes, (3) results in

$$
\begin{aligned}
&k_{nfe}\frac{\partial^2 T_{nf}}{\partial y^2} + h_{sf}a_{sf}\left(T_s - T_{nf}\right) + \frac{16}{3}\frac{\sigma_s T_\infty}{k_e}\frac{\partial^2 T_{nf}}{\partial y^2} + S_{nf} \\
&\quad = \frac{(q_1+q_2)\,u}{Hu_m}
\end{aligned}
\tag{6}
$$

The following nondimensional parameters are introduced to normalize the governing equations and boundary conditions:

$$
\begin{aligned}
U &= \frac{u}{u_m}, \\
Y &= \frac{y}{H}, \\
P &= \frac{K}{u_{nf}u_m}\frac{dp_{nf}}{dx}, \\
N &= \frac{\sigma_{nf}B_0^2H^2}{\rho_{nf}}, \\
Da &= \frac{K}{H^2}; \\
\mathrm{Re} &= \frac{2H\rho_{nf}u_m}{u_{nf}}, \\
\theta &= \frac{k_{se}\left(T-T_{w1}\right)}{q_2H}, \\
s_\varepsilon &= \sqrt{\frac{\varepsilon}{Da}}, \\
\xi &= \frac{q_1}{q_2}, \\
C &= \frac{k_{nfe}}{k_{se}}, \\
w_s &= \frac{S_sH}{q_2}, \\
w_{nf} &= \frac{S_{nf}H}{c_{nf}q_2}, \\
Bi &= \frac{h_{sf}a_{sf}H^2}{k_{se}}
\end{aligned}
\tag{7}
$$

We consider the heat transfer by using the thermophysical properties of nanofluids. Thermal conductivity, dynamic viscosity, density, and magnetic conductivity of nanofluid can be, respectively, correlated with the following formulas:

$$
\begin{aligned}
R_k &= \frac{k_{nf}}{k_f} = 1 + \frac{3\phi\left(k_s/k_f - 1\right)}{\left(k_s/k_f + 2\right) - \phi\left(k_s/k_f - 1\right)} \\
R_\mu &= \frac{\mu_{nf}}{\mu_f} = \frac{1}{(1-\phi)^{2.5}} \\
R_f &= \frac{\sigma_{nf}}{\sigma_f} = 1 + \frac{3\phi\left(\sigma_s/\sigma_f - 1\right)}{\left(\sigma_s/\sigma_f + 2\right) - \phi\left(\sigma_s/\sigma_f - 1\right)} \\
R_\rho &= \frac{\rho_{nf}}{\rho_f} = 1 - \phi + \frac{\phi\rho_s}{\rho_f},
\end{aligned}
\tag{8}
$$

By employing (8) and considering three different concentrations for nanoparticles, such as $\phi = 0\%, 2.5\%, 5\%$, the obtained values for R_k, R_u, R_ρ, and R_f are tabulated in Table 2.

The dimensionless form of the governing equations and boundary conditions can be written as

$$\frac{\partial^2 U}{\partial Y^2} - {s_\varepsilon}^2 U - \frac{R_\rho}{R_\mu}\frac{\varepsilon CI\mathrm{Re}}{2\sqrt{Da}}U^2 - \frac{1}{R_\mu}{s_\varepsilon}^2 P - \frac{R_f}{R_\mu}\varepsilon NU = 0 \quad (9)$$

$$\frac{\partial^2 \theta_s}{\partial Y^2} - Bi\left(\theta_s - \theta_{nf}\right) + w_s = 0 \quad (10)$$

$$R_k C\frac{\partial^2 \theta_{nf}}{\partial Y^2} + Bi\left(\theta_s - \theta_{nf}\right) + w_{nf} = (1+\xi)U \quad (11)$$

$$Y = 0 : U = \beta_V \frac{\partial U}{\partial Y} + A_v \frac{\partial^2 U}{\partial Y^2};$$

$$\theta_S = 0; \quad (12)$$

$$\theta_{nf} = \beta_T \frac{\partial \theta_{nf}}{\partial Y} + A_T \frac{\partial^2 \theta_{nf}}{\partial Y^2};$$

$$Y = 1 : U = -\beta_V \frac{\partial U}{\partial Y} - A_v \frac{\partial^2 U}{\partial Y^2},$$

$$\frac{\partial \theta_s}{\partial Y} + C\frac{\partial \theta_{nf}}{\partial \theta_s} = 1; \quad (13)$$

$$\theta_{nf} = \theta_s - \beta_T \frac{\partial \theta_{nf}}{\partial Y} - A_T \frac{\partial^2 \theta_{nf}}{\partial Y^2}$$

and with the mass conservation equation:

$$\int_0^1 U dY = 1 \quad (14)$$

where

$$\beta_v = \eta_v \frac{2-\sigma_v}{\sigma_v} Kn,$$

$$\beta_T = \eta_T \frac{2-\sigma_T}{\sigma_T}\frac{2\gamma}{\gamma+1}\frac{Kn}{\mathrm{Pr}},$$

$$\frac{Kn\beta_v}{2} = A_v, \quad (15)$$

$$\frac{Kn\beta_T}{2} = A_T.$$

3. Model Solution

For the LTNE model, heat transfer in microchannel with the first-order slip boundary was considered by Xu [16]. The present paper extends the results of previous authors and investigates nanofluid flow and heat transfer with the second-order slip velocity and temperature jump. The situation became complex. In addition, little attention has been given to use the homotopy analysis method to obtain the solution of the LTNE model in all the above-mentioned studies. We obtained explicit analytical solutions and the semianalytical solution of the homotopy analysis in this paper.

3.1. Analytic Solutions. When the inertial constant CI in (9)-(11) is omitted, dimensionless velocity and the temperature of solid and nanofluids with explicit expressions can be obtained as

$$U = \frac{1}{R_\mu}P\left(C_1\cosh\left(\sqrt{\frac{R_f}{R_\mu}\varepsilon N + {s_\varepsilon}^2}Y\right) + C_2 \cdot \sinh\left(\sqrt{\frac{R_f}{R_\mu}\varepsilon N + {s_\varepsilon}^2}Y\right) - \frac{R_\mu {s_\varepsilon}^2}{R_\mu {s_\varepsilon}^2 + R_f\varepsilon N}\right) \quad (16)$$

$$\theta_s = \frac{1}{R_k C + 1}\left\{\frac{P(1+\xi)}{R_f\varepsilon N + R_\mu {s_\varepsilon}^2}\left(C_5\cosh(AY) + C_6 \cdot \sinh(AY)\right) - \frac{-R_\mu}{\left(R_f\varepsilon N + R_\mu {s_\varepsilon}^2\right)/A^2 - R_\mu}\left[C_1 \cdot \cosh\left(\sqrt{\frac{R_f}{R_\mu}\varepsilon N + {s_\varepsilon}^2}Y\right) + C_2 \cdot \sinh\left(\sqrt{\frac{R_f}{R_\mu}\varepsilon N + {s_\varepsilon}^2 Y^2}\right) + \frac{R_\mu {s_\varepsilon}^2}{2\left(R_f\varepsilon N + R_\mu {s_\varepsilon}^2\right)}\left(Y^2 - \frac{2}{A^2}\right)\right] - \left(w_s + w_{nf}\right)\left(\frac{1}{2} \cdot Y^2 - \frac{1}{A^2}\right) - C_3 Y - C_4\right\} + w_s \quad (17)$$

$$\theta_{nf} = \frac{1}{R_k C}\left[-w_s + \frac{(1+\xi)P\left(C_5\cosh(AY) + C_6\sinh(AY)\right)}{\left(R_k C + 1\right)\left(R_f\varepsilon N + R_\mu {s_\varepsilon}^2\right)} + \frac{R_k C + 2}{R_k C + 1}\left(C_3 Y + C_4\right) + \frac{\left(R_k C + 1\right)\left(\left(R_f\varepsilon N + R_\mu {s_\varepsilon}^2\right)/A^2 - R_\mu\right) + R_\mu}{\left(\left(R_f\varepsilon N + R_\mu {s_\varepsilon}^2\right)/A^2 - R_\mu\right)}\left(C_1 \cdot \cosh\left(\sqrt{\frac{R_f}{R_\mu}\varepsilon N + {s_\varepsilon}^2 Y^2}\right) + C_2 \cdot \sinh\left(\sqrt{\frac{R_f}{R_\mu}\varepsilon N + {s_\varepsilon}^2 Y^2}\right)\right) - \left(\frac{R_k C + 2}{R_k C + 1}Y^2 + \frac{2}{A^2}\right)\frac{R_\mu {s_\varepsilon}^2}{2\left(R_f\varepsilon N + R_\mu {s_\varepsilon}^2\right)} + \frac{Y^2}{A^2}\left(\frac{\left(w_s + w_{nf}\right)}{2} - {s_\varepsilon}^2\left(\frac{R_f}{R_\mu}\varepsilon N + {s_\varepsilon}^2\right)\right)\right] \quad (18)$$

where $A = \sqrt{Bi(C+1)/(C+1)}$.

From the mass conservation equation (14), the expression of the dimensionless pressure can be obtained as

$$P = \frac{{s_\varepsilon}^2}{{s_\varepsilon}^2 + \varepsilon N} + \frac{1}{\sqrt{{s_\varepsilon}^2 + \varepsilon N}}\left(\frac{B+Q}{A_1}\right) \tag{19}$$

This can also be expressed:

$$\begin{aligned} P &= \frac{K}{\mu_{nf}u_m}\frac{dp_{nf}}{dx} = \frac{(\triangle P/H)\,K^{1/2}}{\rho_{nf}u_m^2}\frac{\rho_{nf}u_m K^{1/2}}{\mu_{nf}} \\ &= f_K \cdot \mathrm{Re}_K; \end{aligned} \tag{20}$$

where the parameters f_K and Re_K are, respectively, microscopic friction factor and Reynolds number. There the constant parameters A_1, B, and Q are, respectively, as follows:

$$\begin{aligned} A_1 &= \beta_v A_v\left(\sqrt{\frac{R_f}{R_\mu}\varepsilon N + {s_\varepsilon}^2}\right)^3 + 2\beta_v\sqrt{\frac{R_f}{R_\mu}\varepsilon N + {s_\varepsilon}^2} \\ &\cdot \cosh\left(\sqrt{\frac{R_f}{R_\mu}\varepsilon N + {s_\varepsilon}^2}\right) + \left(\frac{R_f}{R_\mu}\varepsilon N + {s_\varepsilon}^2\right)\left(1\right. \\ &+ \beta_v^2\left(\frac{R_f}{R_\mu}\varepsilon N + {s_\varepsilon}^2\right) - A_v^2\left(\frac{R_f}{R_\mu}\varepsilon N + {s_\varepsilon}^2\right)^2\Big) \\ &\cdot \cosh\left(\sqrt{\frac{R_f}{R_\mu}\varepsilon N + {s_\varepsilon}^2}\right) \\ B &= \left(\frac{R_f}{R_\mu}\varepsilon N + {s_\varepsilon}^2\right)\left(-1 + \cosh\left(\sqrt{\frac{R_f}{R_\mu}\varepsilon N + {s_\varepsilon}^2}\right)\right) \\ &\cdot \left(-1 + A_v\left(\frac{R_f}{R_\mu}\varepsilon N + {s_\varepsilon}^2\right)\right. \\ &+ \cosh\left(\sqrt{\frac{R_f}{R_\mu}\varepsilon N + {s_\varepsilon}^2}\right) + A_v\left(\frac{R_f}{R_\mu}\varepsilon N + {s_\varepsilon}^2\right) \\ &+ \cosh\left(\sqrt{\frac{R_f}{R_\mu}\varepsilon N + {s_\varepsilon}^2}\right) \\ &+ \beta_v\sqrt{\frac{R_f}{R_\mu}\varepsilon N + {s_\varepsilon}^2}\sinh\left(\sqrt{\frac{R_f}{R_\mu}\varepsilon N + {s_\varepsilon}^2}\right)\Big) \\ Q &= \left(\frac{R_f}{R_\mu}\varepsilon N + s^2\right)\sinh\left(\sqrt{\frac{R_f}{R_\mu}\varepsilon N + s^2}\right) \\ &\cdot \left(\sinh\left(\sqrt{\frac{R_f}{R_\mu}\varepsilon N + s^2}\right)\right. \\ &+ A_v\left(\frac{R_f}{R_\mu}\varepsilon N + s^2\right)\sinh\left(\sqrt{\frac{R_f}{R_\mu}\varepsilon N + s^2}\right) \\ &+ \sqrt{\frac{R_f}{R_\mu}\varepsilon N + s^2}\beta_v \\ &+ \sqrt{\frac{R_f}{R_\mu}\varepsilon N + s^2}\beta_v\cosh\left(\sqrt{\frac{R_f}{R_\mu}\varepsilon N + s^2}\right)\Big) \end{aligned} \tag{21}$$

According to the boundary condition (12), we can get

$$\begin{aligned} C_1 &= \frac{{s_\varepsilon}^2}{\left(R_f/R_\mu\right)\varepsilon N + {s_\varepsilon}^2} \\ &\cdot \frac{\beta_v\sqrt{\left(R_f/R_\mu\right)\varepsilon N + {s_\varepsilon}^2}\cosh\left(\sqrt{\left(R_f/R_\mu\right)\varepsilon N + {s_\varepsilon}^2}\right) + \left(A_v\left(\left(R_f/R_\mu\right)\varepsilon N + {s_\varepsilon}^2\right) + 1\right)\sinh\left(\sqrt{\left(R_f/R_\mu\right)\varepsilon N + {s_\varepsilon}^2}\right) + \beta_v\sqrt{\left(R_f/R_\mu\right)\varepsilon N + {s_\varepsilon}^2}}{\cosh\left(\sqrt{\left(R_f/R_\mu\right)\varepsilon N + {s_\varepsilon}^2}\right) + \left(-1 - \beta_v{}^2\left(\left(R_f/R_\mu\right)\varepsilon N + {s_\varepsilon}^2\right) + A_v{}^2\left(\left(R_f/R_\mu\right)\varepsilon N + {s_\varepsilon}^2\right)^2\right)\sinh\left(\sqrt{\left(R_f/R_\mu\right)\varepsilon N + {s_\varepsilon}^2}\right)} \end{aligned} \tag{22}$$

$$\begin{aligned} C_2 &= \frac{{s_\varepsilon}^2}{\left(R_f/R_\mu\right)\varepsilon N + {s_\varepsilon}^2} \\ &\cdot \frac{\cosh\left(\left(R_f/R_\mu\right)\varepsilon N + {s_\varepsilon}^2\right) + \beta_v\sqrt{\left(R_f/R_\mu\right)\varepsilon N + {s_\varepsilon}^2}\sinh\left(\sqrt{\left(R_f/R_\mu\right)\varepsilon N + {s_\varepsilon}^2}\right) + A_v\left(\left(R_f/R_\mu\right)\varepsilon N + {s_\varepsilon}^2\right)\cosh\left(\sqrt{\left(R_f/R_\mu\right)\varepsilon N + {s_\varepsilon}^2}\right) + A_v - 1}{-2\beta_v\sqrt{\left(R_f/R_\mu\right)\varepsilon N + {s_\varepsilon}^2}\cosh\left(\sqrt{\left(R_f/R_\mu\right)\varepsilon N + {s_\varepsilon}^2}\right) + \left(-1 - \beta_v{}^2\left(\left(R_f/R_\mu\right)\varepsilon N + {s_\varepsilon}^2\right) + A_v{}^2\left(\left(R_f/R_\mu\right)\varepsilon N + {s_\varepsilon}^2\right)^2\right)\sinh\left(\sqrt{\left(R_f/R_\mu\right)\varepsilon N + {s_\varepsilon}^2}\right)} \end{aligned} \tag{23}$$

Surely, we can get other constant parameters C_3, C_4 C_5, and C_6 by the boundary condition (13). Due to the complex conditions, we need to solve them with Mathematics software. The constant parameters are too long to display in the article. In addition, Nusselt numbers for porous media approach are calculated

$$Nu_1 = \frac{-2\xi}{\theta_{nfb} R_k C},$$
$$Nu_2 = \frac{2}{\left(\theta_{w2} - \theta_{nfb}\right) R_k C} \tag{24}$$

where the bulk mean fluid temperature θ_{nfb} is obtained with

$$\theta_{nfb} = \int_0^1 U\theta_{nf} dY. \tag{25}$$

3.2. Homotopy Solution [22]. From the boundary conditions ((12)-(14)), the initial solution of the equation can be obtained in the following form:

$$U_0 = a_1 \left(2A_V + Y^2 - \frac{2\beta_V + 4A_V + 1}{4\beta_V + 12A_V + 1} Y^4\right),$$
$$a_1 \text{ is a real number;}$$
$$\theta_{s0} = \left(4\beta_T + 2C + 8A_T + 1\right) Y + \left(2C - 2\beta_T + 4A_T\right) Y^2; \tag{26}$$
$$\theta_{f_0} = 2A_T + Y^2;$$

According to the characteristics of the model, the auxiliary linear operators

$$L_U\left[\phi\left(Y;q\right)\right] = \phi'',$$
$$L_{\theta_s}\left[\varphi\left(Y;q\right)\right] = \varphi'', \tag{27}$$
$$L_{\theta_{nf}}\left[\psi\left(Y;q\right)\right] = \psi''$$

$q \in [0,1], \Phi, \varphi, \psi$ are real functions.

According to the basic idea of the homotopy analysis method, the zero-order deformation equations are constructed as follows:

$$\left(1-q\right) L_U\left[\Phi\left(Y;q\right) - U_0\left(Y\right)\right] = q h_U N_U\left[\Phi\left(Y;q\right)\right] \tag{28}$$

$$\left(1-q\right) L_{\theta_s}\left[\varphi\left(Y;q\right) - \theta_s\left(Y\right)\right] = q h_{\theta_s} N_{\theta_s}\left[\varphi\left(Y;q\right), \psi\left(Y;q\right)\right] \tag{29}$$

$$\left(1-q\right) L_{\theta_{\mathrm{nf}}}\left[\psi\left(Y;q\right) - \theta_{\mathrm{nf}}\left(Y\right)\right] = q h_{\theta_{\mathrm{nf}}} N_{\theta_{\mathrm{nf}}}\left[\Phi\left(Y;q\right), \varphi\left(Y;q\right), \psi\left(Y;q\right)\right] \tag{30}$$

where

$$N_U = \frac{d^2\Phi\left(Y;q\right)}{dY^2} - \left(s_\varepsilon{}^2 + \frac{R_f}{R_\mu}\varepsilon N\right)\Phi\left(Y;q\right) - \frac{R_\rho \varepsilon C I \mathrm{Re}}{2R_\mu\sqrt{Da}}\Phi^2\left(Y;q\right) - \frac{1}{R_\mu} s_\varepsilon{}^2 P$$

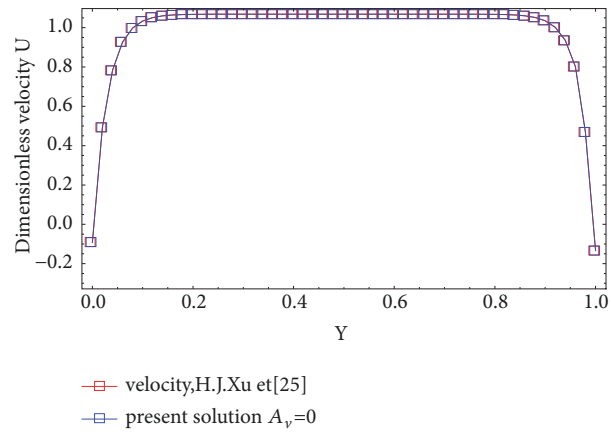

Figure 2: The results of the velocity compared to H. J. Xu. [16].

$$N_{\theta_s} = \frac{d^2\varphi\left(Y;q\right)}{dY^2} - Bi\left(\varphi\left(Y;q\right) - \psi\left(Y;q\right)\right) + w_s$$
$$N_{\theta_{\mathrm{nf}}} = \left(R_k C\right)\frac{d^2\psi\left(Y;q\right)}{dY^2} + Bi\left(\varphi\left(Y;q\right) - \psi\left(Y;q\right)\right) - \left(1+\xi\right)\Phi\left(Y;q\right) + R_c w_{nf} \tag{31}$$

To get the mth-order deformation equations, the zero-order deformations ((28)-(30)) are first differentiated m-times (m=1,2, 3…) with respect to q at q=0 and then the resulting expression is divided by m! so that the m-order deformation equations are shown as follows:

$$L_U\left[U_m\left(Y\right) - \chi_m U_{m-1}\left(Y\right)\right] = h_U R_m^U\left(\overrightarrow{U}_{m-1}\right)$$
$$L_{\theta_s}\left[\theta_{sm}\left(Y\right) - \chi_m\theta_{sm-1}\left(Y\right)\right] = h_{\theta_s} R_m^{\theta_s}\left(\overrightarrow{\theta}_{sm-1}, \overrightarrow{\theta}_{nfm-1}\right) \tag{32}$$
$$L_{\theta_{nf}}\left[\theta_{nfm}\left(Y\right) - \chi_m\theta_{nf\,m-1}\left(Y\right)\right] = h_{\theta_{nf}} R_m^{\theta_{nf}}\left(\overrightarrow{U}_{m-1}, \overrightarrow{\theta}_{sm-1}, \overrightarrow{\theta}_{nfm-1}\right)$$

where

$$\chi_m = \begin{cases} 0, & m \le 1 \\ 1, & m > 1. \end{cases} \tag{33}$$

4. Results and Discussion

We extended the results of H. J. Xu [16] with the first-order slip boundary and investigated nanofluid flow and heat transfer with the second-order slip velocity and temperature jump. Hence, we compared the analytical results for $A_v = 0$, $A_T = 0, \xi = 1$with H. J. Xu et al. [16], as shown in Figure 2. It is worth mentioning that the solution we get is in very good agreement with the result of the paper written by H. J. Xu [16].

The convergence of the HAM solutions depends on the convergence-control parameters h. Figures 3(a) and 3(b) are

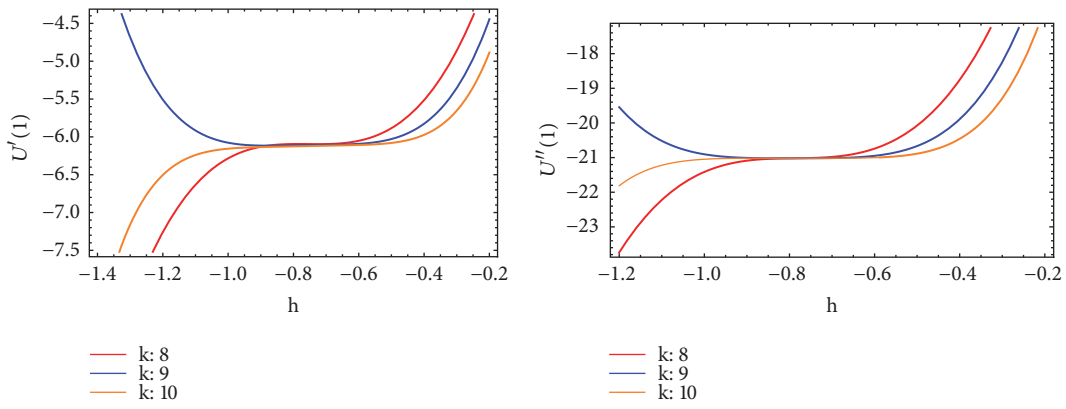

(a) h-curve of $U'(1)$ (b) h-curve of $U''(1)$

Figure 3

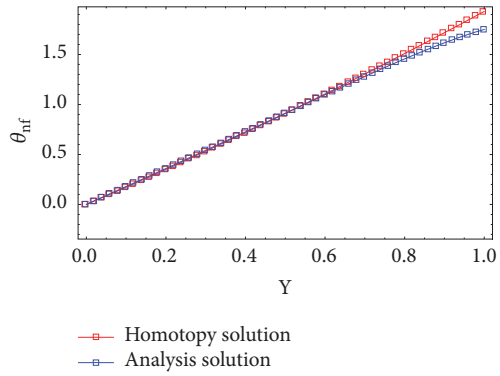

Figure 4: The comparison of two solutions.

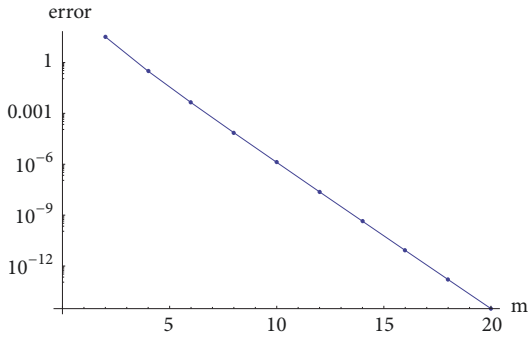

Figure 5: The residual errors of the velocity.

plotted by fixing other parameters to calculate the range of admissible values for the auxiliary parameter h. We find the stable interval of h is about [-0.9, -0.6]. Figure 4 is the comparison of the analytical and homotopy solution. We can see that the solution of the homotopy analysis method coincides with the analytical solution which is obtained. In addition, Figure 5 shows that the error of the model reaches $10^{-12} \sim 10^{-6}$ when the order of the HAM approximation is more than 6-order through BVPh2.0 procedure package with

$$\begin{aligned} CI &= 0, \\ s_\varepsilon &= 3, \\ \frac{\varepsilon CI \mathrm{Re}}{2\sqrt{Da}} &= 0.011, \\ C &= 0.085, \\ Bi &= 0.076, \\ \xi &= 5, \\ \beta_v &= 0.0193, \\ \beta_T &= 0.0235, \\ a_1 &= 0.3. \end{aligned} \tag{34}$$

The effects of slip velocity and temperature jump on velocity and temperature of the solid and nanofluids are showed in Figure 6. In Figure 6(a), the value of first slip velocity coefficient is higher and the velocity distribution is more uniform. It is clear that the first slip velocity coefficient increases; the wall slippage effect is enhanced. This is because the increase in first slip velocity coefficient can be due to increase in the mean free path of the molecules, which in turn decreases the retarding effect at the wall. Figure 6(b) shows the velocity profile at different second slip velocity coefficient. From those curves, the second slip velocity coefficient number increases, the velocity profile shifts up to show increase on the top wall while A_v are opposite effects on velocity of bottom wall. With the temperature jump increases, the temperature of the nanofluids also rises in Figure 6(c). Figure 6(c) also shows that the increase in A_v makes the temperature higher but less symmetrical due to the enhanced local convective heat transfer.

Figures 7(a) and 7(b) show the temperature distributions of the nanofluid phase for varying values of different nanoparticles and nanoparticles volumetric concentration.

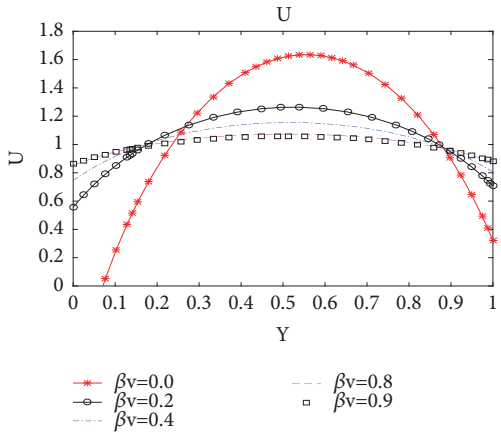

(a) The effect of the first-order slip parameter on U

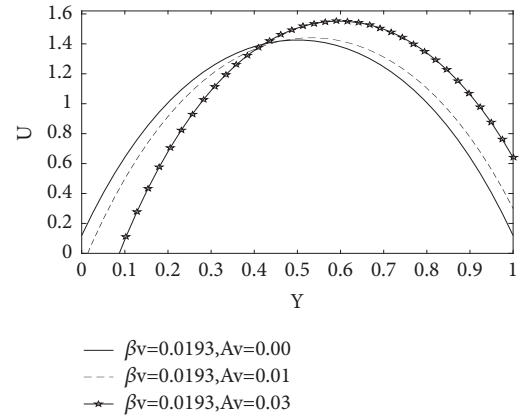

(b) The effect of the second-order slip parameter on U

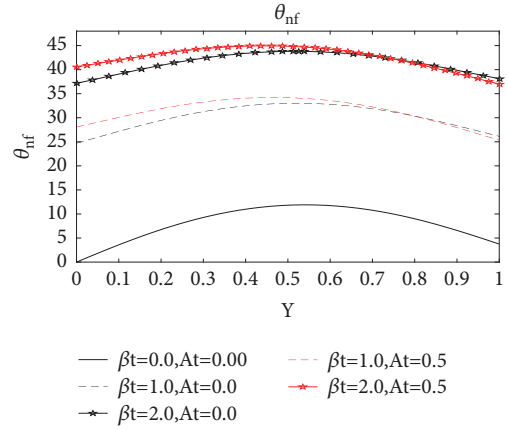

(c) Effect of the second-order temperature jump on θ_{nf}

Figure 6

As a general trend, these figures show that the addition of nanoparticles and variation of their concentration have influences on the temperature of the nanofluid phase. According to temperature plotted in Figure 7(a), it is observed that by increasing the nanoparticle concentration the dimensionless temperature of the nanofluid decreases and gratitude of nanofluid temperature increases. This is in keeping with the physical expectations, as increasing the nanoparticles concentration results in enhancing the thermal conductivity of the nanofluid, which in turn reduces the dimensionless flow temperature. In addition, the gradient of the nanofluids temperature rises gradually while the solid temperature decreases from Table 3 and Figure 7(b). Effects of slip velocity and volume fractions on Nusselt number are presented through Figures 7(c) and 7(d), respectively. Figure 7(c) confirms that, by increasing volume fractions, Nusselt number on bottom wall will be increased. A reverse treatment by increasing the nanoparticles volume fraction is observed through Figure 7(d). Because the Brownian movement carries the heat from the top wall and distributes it to the surroundings, it has the main influence on thermal conductivity of nanofluid. In addition, we find that, by increasing first slip velocity coefficient, Nusselt number on both walls will be increased

Table 3: The effect of the volume fraction on the temperature.

ϕ	s	M	Re	C	$\theta_{nf}'(1)$	$\theta_s'(1)$
0.1	35	0	10	0.085	13.0378	12.8918
0.025 (2.5%)					13.0425	12.8914
0.05 (5%)					13.0471	12.8910

while Nusselt number will be decreased with increasing second slip velocity coefficient.

Figures 8(a) and 8(b) show the temperature profiles of solid and fluid phases for different ratios ξ with $s = 10$, $\varepsilon CI\mathrm{Re}/2\sqrt{Da} = 0.011$, $C = 0.085$, $Bi = 0.076$, $\beta_v = 0.0193$, $\beta_T = 0.0235$, $a_1 = 0.3$, $A_v = 0.0193$, and $A_T = 0.0235$. When ξ becomes larger, the temperature of the nanofluids and solid temperature shifts up due to the faster heat dissipation.

Figure 9 show the development of the nondimensional temperature profiles of the fluid and solid for different magnetic field. As the magnetic felid is stronger, the temperature is larger. At the same time, we can notice that the temperature gets faster on the bottom wall.

Figure 10 shows the temperature for the various Biot numbers. Biot number is the ratio of solid phase conduction

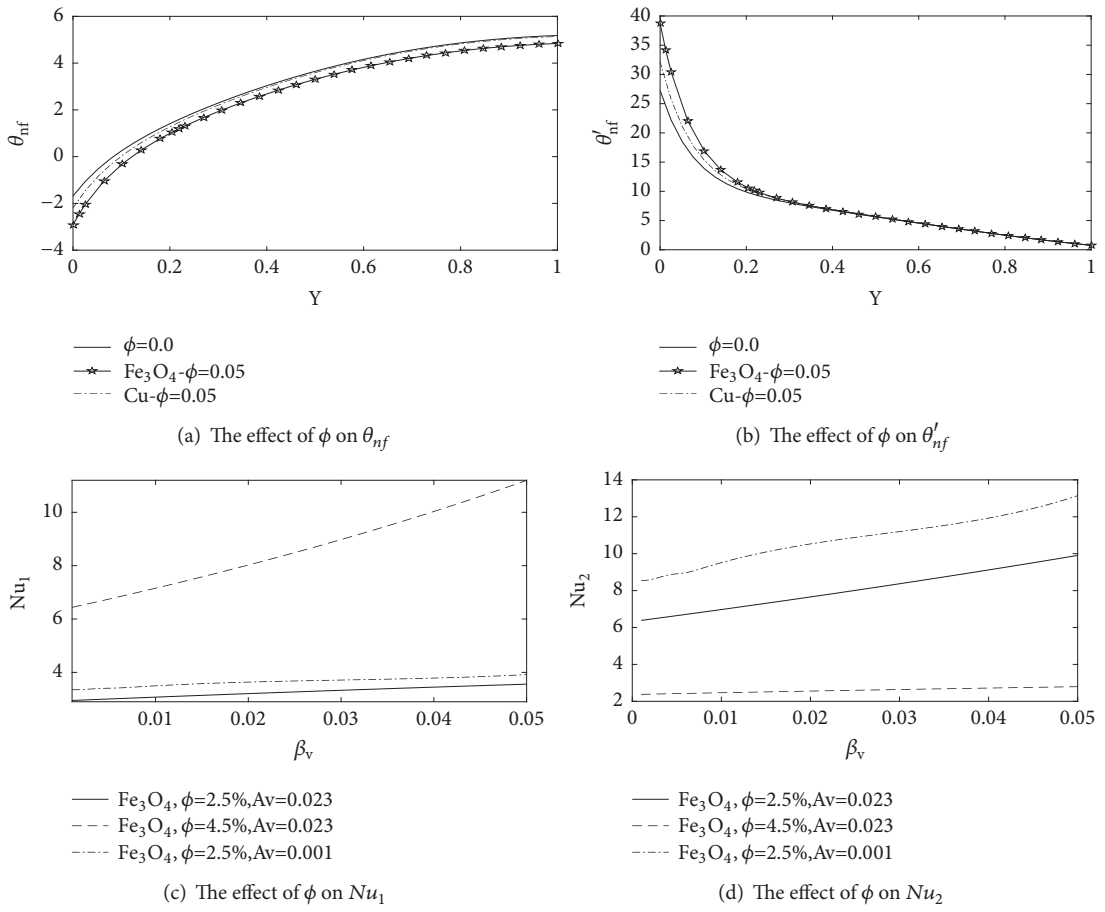

(a) The effect of ϕ on θ_{nf}

(b) The effect of ϕ on θ'_{nf}

(c) The effect of ϕ on Nu_1

(d) The effect of ϕ on Nu_2

Figure 7

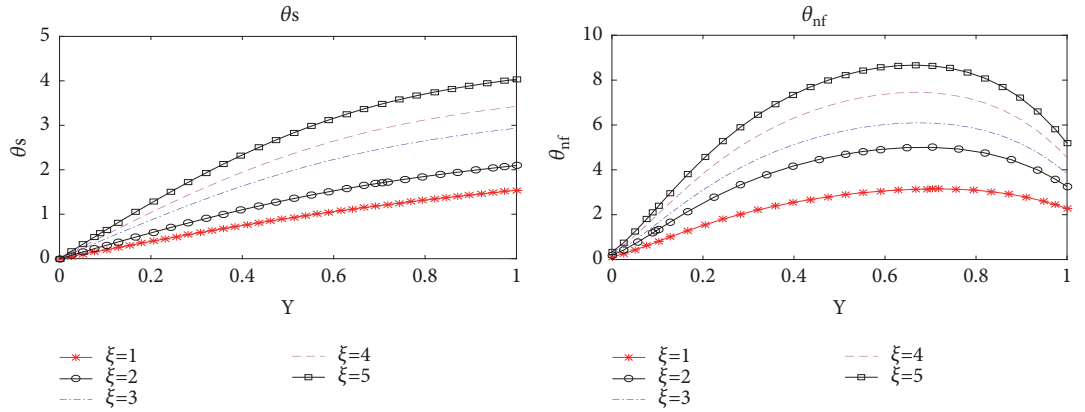

(a) The effect of ξ on θ_S

(b) The effect of ξ on θ_{nf}

Figure 8

resistance over the actual heat exchanged between the fluid and solid phases. According comparisons between solid temperature profiles, the figure shows that the increase in Biot number means to decrease the conduction resistance, so the solid temperature increases and heat transfer can be enhanced by increasing effective Biot number. However, Biot number has opposite effect on nanofluids temperature.

From Figure 11 it can be seen that velocity profile becomes uniform with an increase in shape factor when the boundary conditions are the second-order slip of the velocity. From the H. J. Xu [16], we come to know the figure about s_ε of which the boundary condition is the first-order slip of the velocity and find the trend is too similar. When the shape factor is smaller, the maximal value of the velocity profile is higher.

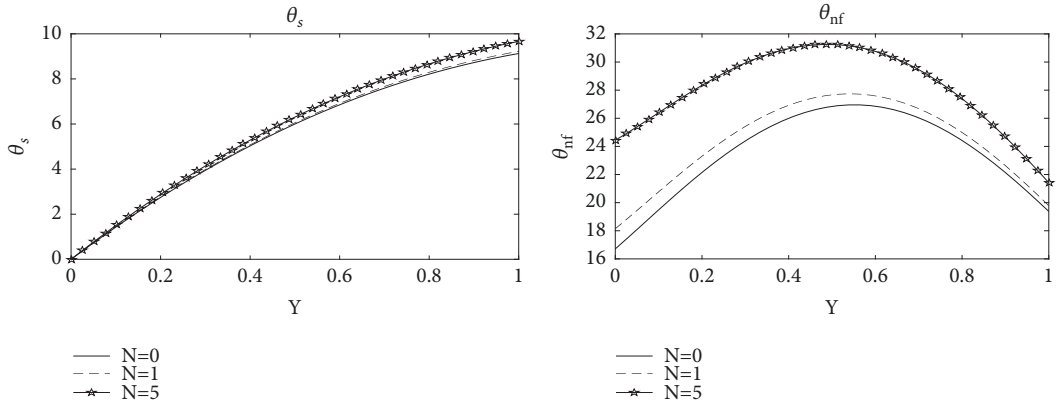

(a) The effect of magnetic felid on θ_S

(b) The effect of magnetic felid on θ_{nf}

Figure 9

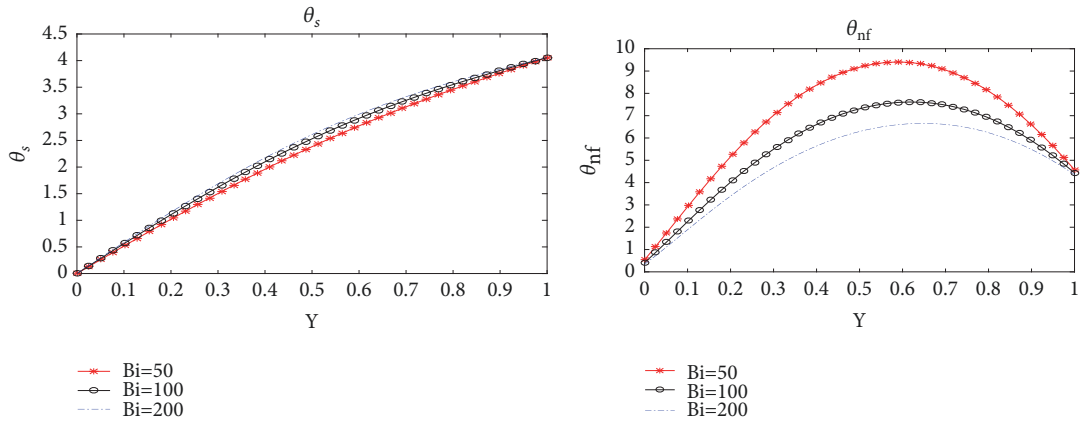

(a) The effect of the Bi on θ_S

(b) The effect of the Bi on θ_{nf}

Figure 10

Figure 12 presents the effect of shape factor on the value for dot product of permeability friction factor and permeability Reynolds number for different Knudsen number. We discuss the small shape factor from 0 to 1. When Knudsen number is small, the value of dimensionless pressure drop first increases and then decreases with the increase in shape factor. Dimensionless pressure drop is sharply decreased for small Knudsen number.

5. Conclusions

Flow and heat transfer for Cu-water and Fe_3o_4-water nanofluid are considered with the composite system including internal heat source, the magnetic field, and the heat flux boundary. Analytical solutions and semianalytical solutions by homotopy analysis are obtained. The present analytical solution agrees well with those previously reported in the literature and HAM solution. The effects of the physical factors on the heat transfer are graphically discussed. The results also show that the first velocity slip enhances Nusselt numbers while the second slip coefficient has a reverse effect on them. Increasing thermal jump coefficient causes the temperature of the nanofluids to rise. Moreover, with the value of the Biot number increasing, the temperature cuts down. The heat transfer enhancement increases with increase of the nanoparticle concentration while it decreases with

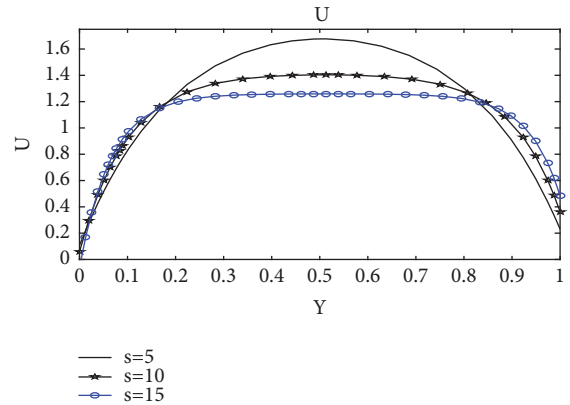

Figure 11: The effect s_ε on the velocity.

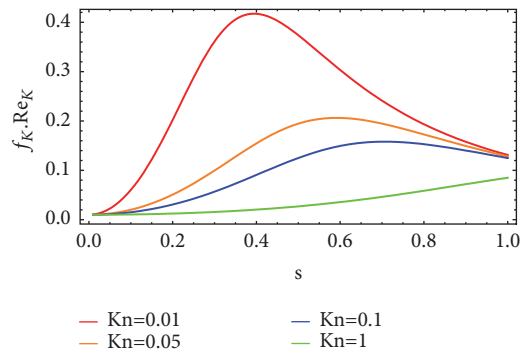

FIGURE 12: Effect of shape factor on $f_K \cdot \mathrm{Re}_K$.

increase of Hartmann number. As expected, the nanoparticle concentration enhances heat transfer on bottom wall. Dimensionless pressure drop is sharply decreased for small Knudsen number.

Nomenclature

CI: Inertial constant
h_{sf}: Convective heat transfer coefficient
μ: Viscosity
p: Pressure
σ: Magnetic conductivity
Bi: Biot number
c: Specific heat capacity
T: Temperature
ϕ: Volume fraction of the solid particles in the nanofluid
x, y: Horizontal and vertical positions
U, V: Dimensionless X, Y velocities
a_{sf}: Specific surface area
K: Permeability
k: Thermal conductivity
q: Heat flux
B_0: Magnetic field intensity
Re: Reynolds number
S: Energy source per unit volume
Da: Darcy number
u, v: Velocity components, respectively, at x, y directions
X, Y: Dimensionless horizontal and vertical positions.

Greek Symbols

β_T, A_T: Thermal slip coefficient
β_v, A_v: Velocity slip coefficient
ε: Porosity
θ: Dimensionless temperature
ξ: HF (heat flux) ratio
ρ: Density
Kn: Knudsen number
Pr: Prandtl number.

Subscripts

1: Bottom plate
2: Upper plate
d: Dispersion
e: Effective/equivalent
nf: Nanofluids
m: Mean
s: Solid
w: Wall
f: Basic fluid.

Data Availability

The data used to support the findings of this study are included within the article.

Conflicts of Interest

The authors declare no conflicts of interest.

References

[1] S. Chol, "Enhancing Thermal Conductivity of Nano fluids with Nanoparticles," *ASME Publications-Fed*, vol. 231, pp. 99–106, 1995.

[2] O. Mahian, A. Kianifar, S. A. Kalogirou, I. Pop, and S. Wongwises, "A review of the applications of nanofluids in solar energy," *International Journal of Heat and Mass Transfer*, vol. 57, no. 2, pp. 582–594, 2013.

[3] M. Lomascolo, G. Colangelo, M. Milanese, and A. De Risi, "Review of heat transfer in nanofluids: Conductive, convective and radiative experimental results," *Renewable & Sustainable Energy Reviews*, vol. 43, pp. 1182–1198, 2015.

[4] M. Ghazvini and H. Shokouhmand, "Investigation of a nanofluid-cooled microchannel heat sink using Fin and porous media approaches," *Energy Conversion and Management*, vol. 50, no. 9, pp. 2373–2380, 2009.

[5] M. Hatami and D. D. Ganji, "Thermal and flow analysis of microchannel heat sink (MCHS) cooled by Cu-water nanofluid using porous media approach and least square method," *Energy Conversion and Management*, vol. 78, pp. 347–358, 2014.

[6] M. Hosseini, E. Mohammadian, M. Shirvani, S. N. Mirzababaei, and F. S. Aski, "Thermal analysis of rotating system with porous plate using nanofluid," *Powder Technology*, vol. 254, pp. 563–571, 2014.

[7] A. J. Chamkha, A. M. Rashad, C. R. Reddy, and P. V. S. N. Murthy, "Viscous dissipation and magnetic field effects in a non-darcy porous medium saturated with a nanofluid under convective boundary condition," *Special Topics and Reviews in Porous Media*, vol. 5, no. 1, pp. 27–39, 2014.

[8] C. Zhao, S. Tassou, and T. Lu, "Analytical considerations of thermal radiation in cellular metal foams with open cells," *International Journal of Heat and Mass Transfer*, vol. 51, no. 3-4, pp. 929–940, 2008.

[9] T. Özgümüş, M. Mobedi, Ü. Özkol, and A. Nakayama, "Thermal dispersion in porous media—a review on the experimental studies for packed beds," *Applied Mechanics Reviews*, vol. 65, no. 3, p. 031001, 2013.

[10] O. M. Haddad, M. M. Abuzaid, and M. A. Al-Nimr, "Developing Free-Convection Gas Flow in a Vertical Open-Ended Microchannel Filled with Porous Media," *Numerical Heat Transfer, Part A: Applications*, vol. 48, no. 7, pp. 693–710, 2005.

[11] M. Nojoomizadeh, A. Karimipour, M. Firouzi, and M. Afrand, "Investigation of permeability and porosity effects on the slip

velocity and convection heat transfer rate of Fe3O4/water nanofluid flow in a microchannel while its lower half filled by a porous medium," *International Journal of Heat and Mass Transfer*, vol. 119, pp. 891–906, 2018.

[12] K. Zheng, Q. Sun, and M. Ni, "Local Non-Equilibrium Thermal Effects in Solid Oxide Fuel Cells with Various Fuels," *Energy Technology*, vol. 1, no. 1, pp. 35–41, 2013.

[13] M. Esfandiary, B. Mehmandoust, A. Karimipour, and H. A. Pakravan, "Natural convection of Al2O3-water nanofluid in an inclined enclosure with the effects of slip velocity mechanisms: Brownian motion and thermophoresis phenomenon," *International Journal of Thermal Sciences*, vol. 105, pp. 137–158, 2016.

[14] B. Buonomo, O. Manca, and G. Lauriat, "Forced convection in micro-channels filled with porous media in local thermal non-equilibrium conditions," *International Journal of Thermal Sciences*, vol. 77, pp. 206–222, 2014.

[15] K. Hooman, "Slip flow forced convection in a microporous duct of rectangular cross-section," *Applied Thermal Engineering*, vol. 29, no. 5-6, pp. 1012–1019, 2009.

[16] H. J. Xu, C. Y. Zhao, and Z. G. Xu, "Analytical considerations of slip flow and heat transfer through microfoams in mini/microchannels with asymmetric wall heat fluxes," *Applied Thermal Engineering*, vol. 93, pp. 15–26, 2016.

[17] S. Sivasankaran, M. A. Mansour, A. M. Rashad, and M. Bhuvaneswari, "MHD mixed convection of Cu–water nanofluid in a two-sided lid-driven porous cavity with a partial slip," *Numerical Heat Transfer, Part A: Applications*, vol. 70, no. 12, pp. 1356–1370, 2016.

[18] P. A. Thompson and S. M. Troian, "A general boundary condition for liquid flow at solid surfaces," *Nature*, vol. 389, no. 6649, pp. 360–362, 1997.

[19] A. Beskok and G. E. Karniadakis, "A model for flows in channels, pipes, and ducts at micro and nano scales," *Nanoscale and Microscale Thermophysical Engineering*, vol. 3, no. 1, pp. 43–77, 1999.

[20] J. Zhu, D. Yang, L. Zheng, and X. Zhang, "Effects of second order velocity slip and nanoparticles migration on flow of Buongiorno nanofluid," *Applied Mathematics Letters*, vol. 52, pp. 183–191, 2016.

[21] S. G. Kandlikar, S. Garimella, D. Q. Li, S. Colin, and M. R. King, *Heat Transfer and Fluid Flow in Minichannels and Microchannels*, Elsevier Science, 2005.

[22] S. J. Liao, *The Proposed Homotopy Analysis Techniques for The Solution of Nonlinear Problem[D]*, Shanghai Jiao Tong University, Shanghai, China, 1992.